Protein-nanocrystal conjugates support a single filament polymerization model in R1 plasmid segregation*

Charina L. Choi[1,2], Shelley A. Claridge[1,2], Ethan C. Garner[3], A. Paul Alivisatos[1,2], R. Dyche Mullins[3]
From the [1]Department of Chemistry, University of California, Berkeley, CA 94720, USA, [2]Material Sciences Division, Lawrence Berkeley National Laboratory, Berkeley, CA 94720, USA
and the [3]Department of Cellular and Molecular Pharmacology, University of California, San Francisco, CA 94143, USA.
Running head: Ultrastructure of Plasmid Segregation Machinery
Address correspondence to: R. Dyche Mullins, 600 16th Street, San Francisco, CA 94143-5800. Fax: 415-514-0133; E-mail: dyche@mullinslab.ucsf.edu

Summary

To ensure inheritance by daughter cells, many low-copy bacterial plasmids, including the R1 drug-resistance plasmid, encode their own DNA segregation systems. The *par* operon of plasmid R1 directs construction of a simple spindle structure which converts free energy of polymerization of an actin-like protein, ParM, into work required to move sister plasmids to opposite poles of rod-shaped cells. The structures of individual components have been solved but little is known about the ultrastructure of the R1 spindle. To determine the number of ParM filaments in a minimal R1 spindle, we used DNA-Au nanocrystal conjugates as mimics of the R1 plasmid. We find that each end of a single polar ParM filament binds to a single ParR/*parC*-Au complex, consistent with the idea that ParM filaments bind in the hollow core of the ParR/*parC* ring complex. Our results further suggest that multi-filament spindles observed in vivo are associated with clusters of plasmids segregating as a unit.

Introduction

In eubacteria and archaea, many biologically important processes are carried out by genes encoded on large, low-copy plasmids. These include genes conferring resistance to antibiotic and heavy metal toxicity as well as genes involved in host cell invasion and pathogenicity. These large plasmids face a difficult challenge. To reduce the metabolic load they impose on the host cell, their copy numbers must be kept to a minimum (1-2 per chromosome equivalent) (1). At such low copy numbers they can no longer rely on chance for their maintenance in the bacterial population. To be stably maintained, these low-copy plasmids must – like chromosomes – be actively segregated to daughter cells before division. Two classes of plasmid segregation systems (Type I and Type II) have been known and studied for years (2) and recent work has uncovered several more (3,4). Each system appears to be encoded on a single operon and to be composed of three pieces: 1) a centromeric DNA sequence; 2) a DNA binding protein; and 3) a polymer-forming protein. The most well-understood of these systems is the Type II segregation machinery encoded by the R1 drug resistance plasmid. Segregation of R1 is driven by the *par* operon, which consists of a 150 bp centromeric sequence (*parC*), a repressor protein (ParR) which binds to the centromeric sequence, and a divergent actin-like protein (ParM) that polymerizes into dynamically unstable filaments in the presence of ATP (5). Binding of the ParR/*parC* complex to ParM filaments stabilizes them against catastrophic disassembly and promotes their elongation via insertional polymerization at the interface with the ParR/*parC* complex. When both ends of a ParM filament are bound to ParR/*parC* complexes, elongation of the filament pushes the attached plasmids in opposite directions.

High-resolution structures of components of the R1 spindle are available (6, 7), but provide little information about the ultrastructure of the R1 spindle itself. The atomic structure of ParM monomers reveals a basic similarity to conventional actin while electron microscopy reveals that ParM and actin filaments differ significantly (8). Like actin, ParM filaments are structurally polarized, with distinct ends corresponding to the barbed and pointed ends of

a conventional actin filament. Unlike actin, the long-pitch, two-start helix of ParM filaments is left-handed rather than right-handed and the orientation of the ParM monomer with respect to the filament axis is significantly different from that of actin. Both free and ParR/*parC*-bound filaments elongate at equal rates from each end. This fact and the polar nature of ParM filaments place constraints on the mechanism of the interaction with the ParR/*parC* complex. Either: a) ParR/*parC* contains two distinct ParM binding sites, one for 'pointed' ends and one for 'barbed'; b) spindles are composed of bundles of anti-parallel filaments, and the complex recognizes an identical surface at each end of the bundle; or c) ParR/*parC* interacts with a surface present at or near both filament ends.

X-ray crystallography of the ParR/*parC* complex reveals that multiple ParR dimers assemble into a helical ring with *parC* DNA running around the outside edge. This "segrosome" ring is hollow, with a 6 nm hole through the center. The size of the hole suggests that a single ParM filament (also 6 nm in diameter) might bind the inside of the ParR/*parC* ring complex (6,7). By forming a collar around the end of a filament the ParR/*parC* complex would pose no barrier to elongation and, if the affinity of the complex for ParM depends on the nucleotide bound to the filament, hydrolysis of ATP within the filament could promote tracking of the complex with the elongating filament end. This is similar to the way in which the Dam1 complex is thought to interact with the dynamic ends of microtubules (9). In addition, a collar encircling a ParM filament might prevent monomer dissociation, providing an attractive explanation for how the ParR/*parC* complex stabilizes filaments against catastrophic disassembly. This model appears to be at odds with *in vivo* studies of R1 spindles that suggest plasmids are segregated by spindles composed of multiple filaments (10). R1 plasmids, however, are also observed to cluster *in vivo* and it is unclear whether multi-filament spindles observed *in vivo* are assembled by pairs of individual plasmids or by pairs of plasmid clusters.

To better understand the coupling of the ParR/*parC* complex to ParM filaments we determined the maximum number of filaments that can simultaneously associate with an individual ParR/*parC* complex. To do this we attached defined numbers of *parC*-containing DNA molecules to gold (Au) nanoparticles and counted the number of filaments associated with each particle. Preparation of such discrete DNA-Au particles is well established (11, 12). We initiated ParM filament formation *in vitro* in the presence of DNA-Au nanoparticle conjugates and visualized associated ParM filaments by transmission electron microscopy (TEM). The high contrast of Au nanoparticles enabled us to identify the location of ParR/*parC* complexes relative to ParM filaments.

Experimental Procedures

Preparation of Au colloid—Samples of 5 and 10 nm Au colloid were prepared according to a literature procedure (13), described in detail in Claridge et al. (14). The Au particles were used as an electron-dense tag for *parC* strands.

Hybridization of thiolated double-stranded parC DNA—The 150 bp *parC* was composed of four oligos (synthesized, purified by polyacrylamide gel electrophoresis, Integrated DNA Technologies, Coralville, IA) as shown in Fig. 1A. The following oligo sequences were used (cpc1 denotes the strand containing the cp and c1 regions; p2 denotes the srand containing the p and 2 regions):

c2: 5'- (thiol) – TTT TTG GTG TTT TTT TGG TGT GTG TTT GGG TAT GTT TTG GGT TTT AAA TGG GTT TGT TTG-3'

cpc1: 5'-TCA AGT TTA CCC CAT TTC AAC CAT CAA TCA ATG ATT ATT TGT CTT GTT TTG GTG TTT TAT TGG GTT GGG TAT GGG TTG TTT TTG GGT TTT GTT TAA AAA-3'

1: 5'-TTT TTA AAC AAA ACC CAA AAA CAA CCC ATA CCC AAC CCA ATA AAA CAC CAA AAC AAG ACA-3'

p2: 5'-AAT AAT CAT TGA TTG ATG GTT GAA ATG GGG TAA ACT TGA CAA ACA AAC CCA CTT AAA ACC CAA AAC ATA CCC AAA CAC ACA CCA AAA AAA CAC C-3'

A solution with 6 μM in each of the four oligos in 100 mM NaCl was heated at 80°C for 2 min, then cooled to room temperature over one hour to allow the strands to hybridize.

Synthesis of parC-Au Conjugates—DNA-Au conjugates were prepared and isolated according to Zanchet et al. (11) and Loweth et al. (13). A 3% agarose gel was used to separate different types of conjugates.

Protein Purification—Untagged ParM and ParR were purified following procedures described by Garner et al. (15).

Mixing of parC-Au conjugates with other Par components and ATP—ParM and ParR were diluted to 23 μM and 2 μM, respectively, in Buffer F (100 mM KCl, 30 mM tris-HCl (pH 7.5), 1 mM $MgCl_2$, and 1 mM TCEP). A 20 μL solution of 15-30 nM *parC*-Au, 350-700 nM ParR, and 2.3 uM ParM in Buffer F/FA (1% w/v 400 cP methyl cellulose, 100 mM KCl, 30 mM tris-HCl (pH 7.5), 1 mM $MgCl_2$, and 500 μM tris(2-carboxyethyl)phosphine-HCl (TCEP)) (15) was mixed and incubated on ice for 10-20 min while TEM grids were plasma ionized. The sample was pipetted onto a strip of parafilm, and 1.5 μL ATP (100 mM) was added for a total of 15-60 s to initiate ParM polymerization. Experiments without ParR were performed similarly, but with Buffer F in place of ParR to maintain similar sample volume and salt concentration. Control experiments of *parC*-Au particles alone, all components without ParM, and all components without ATP were performed, with no filaments observed in any of these cases (Fig. S1). Occasionally gray wisps of around 50 nm length attached to the Au particles were observed, in all control cases, leading us to hypothesize that the wisps are *parC*-Au strands. These occasional observations were not surprising; uranyl acetate is a known stain for large DNA sequences, but DNA on the order of hundreds of base pairs (such as *parC*) is more difficult to visualize.

Preparation and visualization of samples by transmission electron microscopy—Carbon-coated copper TEM grids (Ted Pella) were ionized for 30 s in a Harrick Plasma PDC-32G oxygen plasma cleaner to increase surface hydrophilicity; the grids were then floated carbon-side down for 1-10 s on the 15 μL sample + 1.5 μL ATP (10 mM) reaction. The sample was wicked off and allowed to partially air dry. Once grids were nearly dry, 10 μL of 2% uranyl acetate was added to each grid and incubated for 1 minute. The uranyl acetate stain was wicked off, and the grids were then immersed sequentially in two 50 mL tubes of deionized water for a total of 50 s. The water was wicked off and grids were allowed to air dry prior to analysis. Transmission electron microscopy was performed using a Phillips Tecnai G^2 20.

Determination of normalized structure occurrence—Wide-field images (19.5k to 38k magnification) for experiments with and without ParR were analyzed and the observed structures on each image (Au-M-Au, Au-M, M with Au close to end, M with Au close to side, M alone) were counted manually. The normalized structure occurrence was obtained by dividing the number of that structure type by the total number of structures observed; normalized occurrence for experiments with and without ParR were tabulated separately.

Measurement of ParM filament width in Au-M and Au-M-Au structures—Images (38k to 97k magnification) of Au-M structures (53 total) and Au-M-Au structures (27 total) were analyzed using NIH ImageJ image analysis software (http://rsb.info.nih.gov/ij/). A line scan perpendicular to the length of each ParM filament yielded a plot of pixel intensity vs. distance; the distance between the darkest points of the scan was taken to be the filament width. Five line scans for each filament were taken at different points along the filament and the mean of the resulting widths was taken to be the average width of the filament. The histograms for each type of structure were obtained by binning the widths: widths of $4.5 < x \leq 5.5$ nm were binned as 5 nm, and so on, up to 8 nm.

Results

Garner et al. (15) found that, in the presence of ParR, polystyrene particles conjugated to hundreds of copies of *parC* DNA stabilized bundles of up to 100 ParM filaments. To determine the number of ParM filaments that interact with a single ParR/parC complex we prepared Au particles conjugated to single copies of *parC*-containing DNA, an established and well-characterized procedure (11, 12). Briefly, we incubated Au particles with thiolated *parC*-containing DNA to obtain particles conjugated to zero, one, two, or three *parC*

sequences. We separated different sized conjugates by gel electrophoresis (Fig. 1B); excised bands containing individual, conjugated species from the gel; and extracted and purifed the monoconjugated particles.

We mixed monoconjugate *parC*-Au (Fig. 2A) with purified ParR and ParM, added ATP to induce filament formation, and observed the resulting structures by TEM. We then quantitated the specific association between ParM filaments and *parC*-Au monoconjugates by comparing and counting the types of structures observed in the absence and presence of the DNA-binding protein ParR (Fig. 2I). In the absence of ParR we rarely observed gold particles associated with ParM filaments (Fig. 2H) while, in the presence of ParR, we often observed gold particles closely associated with one or both ends of a ParM structure, with no observable gap between the filament and the Au particle. Addition of ParR increased the frequency with which Au particles associated with one end of a ParM filament structure (Au-M) (Fig. 2, D and E) by more than five fold (Fig. 2I). Likewise, in the presence of ParR we observed ParM structures capped on both ends with an Au particle (Au-M-Au) (Fig. 2, B and C) but never observed such Au-M-Au structures in the absence of ParR (Fig. 2I). These data indicate that the majority of the Au-M and all of the Au-M-Au structures seen in the presence of ParR represent *parC*-Au nanoparticles bound specifically to ParM filaments via ParR.

We also observed Au particles in proximity to the end or side of ParM filaments but separated by an observable gap (Fig. 2, F and G). We scored all such cases in which Au particles were within 15 nm of a ParM filament and found that they occurred with equal frequency in the absence and presence of ParR, suggesting that they represent chance proximity between filaments and particles (Fig. 2I). The majority of ParM filaments in the absence and presence of ParR were not colocalized with Au particles (Fig. 2H). This is reasonable since we used 2.3 μM ParM, a concentration at which filaments can form spontaneously (15).

To determine the number of filaments bound to an individual ParR/*parC* complex we measured the width of the ParM filaments in Au-M and Au-M-Au structures. In both cases we measured an average width of 6.0 ± 0.6 nm, in good agreement with the width of single ParM filaments (16, 17) (Fig. 3). We never observed ParM structures greater than 8 nm in width, indicating that none of the observed structures (n=80) contained two filaments.

We observed singly capped filaments more frequently than doubly capped, consistent with a lower probability that a ParM filament will encounter two ParR/*parC*-Au complexes compared to one. The optimal ParM concentration for electron microscopy was approximately 2.5 μM. At higher concentrations (7-15 μM, near the ParM concentration estimated inside R1-containing bacterial cells) the filament density was too high to accurately distinguish capped from uncapped filaments. We also tried assembling spindles at high concentration and diluting them immediately prior to visualization but found that the filaments were sheared and broken by pipetting. At lower concentrations (approaching 0.6 μM, the critical concentration for ATP ParM filaments (15)) we observed capped filaments but with significantly reduced frequency.

Attempts to increase the encounter frequency by increasing the concentration of *parC*-Au/ParR particles in solution resulted in a density of Au particles too high to distinguish individual Au-M and Au-M-Au structures.

To determine whether our failure to observe more than one ParM filament per Au particle reflects the binding capacity of the ParR/*parC* complex or an experimental artifact, we mixed ParM with Au nanoparticles conjugated to four or more *parC* sequences (Fig. 4A). In the presence of ParR and ATP the multi-conjugated Au particles associated with the ends of bundles composed of up to six ParM filaments (Fig. 4, B to E). These data argue strongly that our results with monoconjugated Au particles reflect the binding capacity of the ParR/*parC* complex. The occurrence of multi-filament spindles under these conditions is consistent with our previous observation of multi-filament spindles formed by multi-conjugated particles (15) and suggests that, once a single-filament spindle is formed, the probability of the tethered particles capturing additional filaments is relatively high.

Discussion

DNA-Au nanoparticle conjugates have been used for a variety of purposes, including nanoparticle self-assembly (14) and as probes of biomolecular dynamics (18). For small Au nanoparticles (less than 15 nm in diameter) and DNA oligos longer than 100 bp, it is straightforward to tune the number of DNA molecules attached to each particle (11, 12). Our *in vitro* results using DNA-Au monoconjugates to mimic the R1 plasmid demonstrate that a single ParR/*parC* complex binds either end of a single ParM filament. This implies that, *in vivo*, pairs of plasmids are segregated by polymerization of single ParM filaments. This is consistent with what is known about the physical properties of ParM filaments. Theoretical considerations and measurements of force produced by polymerizing actin filaments suggest that, *in vivo*, a growing ParM filament can generate forces on the order of 1 pN (19). Stiffness measurements (our unpublished observations) indicate that ParM filaments have a persistence length (~10 μm) several times longer than the length of a bacterial cell (1-3 μm) and that, at bacterial length scales, ParM filaments require pN forces to buckle. These forces are several orders of magnitude greater than those required to push plasmids through bacterial cytoplasm (20).

Taken together with recent structural studies of the ParR/*parC* complex (6,7) our results suggest that a single 6 nm diameter ParM filament might fit within the ParR segrosome ring. This arrangement would explain three important experimental observations regarding ParM polymer dynamics. By forming a collar around the ParM filament rather than binding the end of the filament 'face on,' the ParR/*parC* ring: 1) could interact with identical surfaces at either end of a ParM filament; 2) would not be expected to affect the elongation rate of bound ParM filaments; and 3) could interact with no more than one filament at a time. One hypothesis for how the ParR/*parC* rings surf on the growing ends of ParM filaments would, thus, be that the ring has high affinity for ATP-bound portions of the filament and lower affinity for portions of the filament that have hydrolyzed bound ATP (15). An appealing analogy for this situation is the way in which Dam1 complexes are thought to encircle microtubules. Dam1 rings appear to prefer the plus end of a microtubule but, by applying force to the complex, it can be moved away from the tip and slide along the entire length of the microtubule (21). Additional single molecule experiments will be required to determine whether this is also true for ParR/parC rings.

Finally, we previously found that, *in vivo*, R1 spindles are occasionally composed of at least two ParM filaments (10). Our results using monoconjugate Au particles suggest that these multi-filament spindles contain at least two ParR/*parC* complexes at each end. This implies that clusters composed of multiple plasmids (22) can segregate together as a single unit *in vivo*. This is also consistent with our previous observations of plasmid dynamics in vivo. Using plasmids labeled with fluorescently tagged DNA-binding proteins we often observed segregation of plasmid foci with dramatically different fluorescence intensities (10), suggesting that the two foci contained different numbers of plasmids. Plasmid clustering is not well understood but we suggest that it may play a previously unsuspected role in replication and segregation *in vivo*.

Acknowledgements

We thank C. S. Campbell for protein preparation and helpful discussion.

References

1. Nordström, K., Ingram, L. C., Lundbäck, A. (1972) *J. Bacteriol.* **110**, 562-569.
2. Gerdes, K., Møller-Jensen, J., Bugge Jensen, R. (2000) *Mol Microbiol.* **37**, 455-466.
3. Larsen, R. A., Cusumano, C., Fujioka, A., Lim-Fong, G., Patterson, P., Pogliano, J. (2007) *Genes Dev.* **21**, 1340-1352.
4. Becker, E., Herrera, N. C., Gunderson, F. Q., Derman, A. I., Dance, A. L., Sims, J., Larsen, R. A., Pogliano, J. (2006) *EMBO J.* **25**, 5919-5931.
5. Møller-Jensen, J., Jensen, R. B., Löwe, J., Gerdes, K. (2002) *EMBO J.* **21**, 3119-3127.
6. Møller-Jensen, J., Ringgaard, S., Mercogliano, C. P., Gerdes, K., Lowe, J. (2007) *EMBO J.* **26**, 4413-4422.
7. Schumacher, M. A., Glover, T. C., Brzoska, A. J., Jensen, S. O., Dunham, T. D., Skurray, R. A., Firth, N. A. (2007) *Nature* **450**, 1268-1272.
8. Orlova, A., Garner, E. C., Galkin, V. E., Heuser, J., Mullins, R. D., Egelman, E. H. (2007) *Nat. Struct. Mol. Biol.* **14**, 921-926.
9. Westermann, S., Wang, H. W., Avila-Sakar, A., Drubin, D. G., Nogales, E., Barnes, G. (2006) *Nature* **440**, 565-569.
10. Campbell, C. S. and Mullins, R. D. (2007) *J. Cell Biol.***179**, 1059-1066.
11. Zanchet, D., Micheel, C. M., Parak, W. J., Gerion, D., Alivisatos, A. P. (2001) *Nano Lett.* **1**, 32 -35.
12. Claridge, S. A., Liang, H. W., Basu, S. R., Frechet, J. M. J., Alivisatos, A. P. (2008) *Nano Lett.* **8**, 1202-1206.
13. Loweth, C. J., Caldwell, W. B., Peng, X. G., Alivisatos, A. P., Schultz, P. G. (1999) *Angew. Chem. Int. Ed.* **38**, 1808-1812.
14. Claridge, S. A., Goh, S. L., Frechet, J. M. J., Williams, S. C., Micheel, C. M., Alivisatos, A. P. (2005) *Chem. Mater.* **17**, 1628-1635.
15. Garner, E. C., Campbell, C. S., Weibel, D. B., Mullins, R. D. (2007) *Science* **315**, 1270 -1274.
16. Garner, E. C., Campbell, C. S., Mullins, R. D. (2004) *Science* **306**, 1021-1025.
17. van den Ent, F., Møller-Jensen, J., Amos, L. A., Gerdes, K., Löwe, J. (2002) *EMBO J.* **21**, 6935-6943.
18. Sönnichsen, C., Reinhard, B.M., Liphardt, J., Alivisatos, A. P. (2005) *Nat. Biotechnol.* **23**, 741-745.
19. Dye, N. A., Shapiro, L. (2007) *Trends in Cell Biol.* **17**, 239-245.
20. Giardini, P. A., Fletcher, D. A., Theriot, J. A. (2003) *Proc. Natl. Acad. Sci. USA* **100** 6493-6498.
21. Ashbury, C. L., Gestaut, D. R., Powers, A. F., Franck, A. D., Davis, T. N. (2006) *Proc. Natl. Acad. Sci.* **103**, 9873-9878.
22. Pogliano, J., Ho, T. Q., Zhong, Z., Helinski, D. R. (2001) *Proc. Natl. Acad. Sci. USA* **98**, 4486-4491.

Footnotes

***** This paper was supported by the UCSF/UCB Nanomedicine Development Center NIH Grant No. PN2 EY016546 as administered through UCSF, and by grants to RDM from the Sandler Family Supporting Foundation and the National Institutes of Health (5R01GM079556-03), and by the Director, Office of Science, Office of Basic Energy Sciences, of the U.S. Department of Energy under Contract No. DE-AC02-05CH11231. This document was prepared as an account of work sponsored by the United States Government. While this document is believed to contain correct information, neither the United States Government nor any agency thereof, nor The Regents of the University of California, nor any of their employees, makes any warranty, express or implied, or assumes any legal responsibility for the accuracy, completeness, or usefulness of any information, apparatus, product, or process disclosed, or represents that its use would not infringe privately owned rights. Reference herein to any specific commercial product, process, or service by its trade name, trademark, manufacturer, or otherwise, does not necessarily constitute or imply its endorsement, recommendation, or favoring by the United States Government or any agency thereof, or The Regents of the University of California. The views and opinions of authors expressed herein do not necessarily state or reflect those of the United States Government or any agency thereof or The Regents of the University of California.

Figure legends

Figure 1. Au particles conjugated to defined numbers of *parC*-containing, double-stranded DNA molecules are prepared by covalent thiol-Au attachment and separated by gel electrophoresis. (A) The 150 bp *parC* construct consists of two regions (1 and 2), with a promoter (p) region in-between; c1, cp, and c2 denote the corresponding regions on the complementary strand. To incorporate a thiol group at one end of the construct, we used synthesized DNA. Each *parC* strand was divided into two parts (shown schematically as gray and black) for a total of four synthesizable oligos. The four oligos were hybridized together before conjugation to Au particles. (B) Conjugation of thiolated *parC* to Au particles results in a mixture of particles with different numbers of *parC* attached. The mixture was run in a 3% agarose gel to separate different types of conjugates. Particles conjugated to different numbers of *parC* sequences were then excised from the gel and extracted. Left lane: Au particles alone. Right lane: Au particles conjugated with DNA; separation of Au particles with 0, 1, 2, and 3 DNA strands attached is clearly shown.

Figure 2. Individual *parC*-Au/ParR complexes attach to one or both ends of a single ParM filament. (A) Monoconjugate *parC*-Au (schematic) was used as an R1 plasmid mimic to investigate the number of ParM filaments which would bind to a single *parC*. (B)-(C) Single ParM filaments with a *parC*-Au/ParR complex at both filament ends (Au-M-Au). (D)-(E) Single ParM filaments with a *parC*-Au/ParR complex at one filament end (Au-M). (F) ParM filaments with a *parC*-Au particle close to but separated from the filament end (M with Au close to end) were observed with near equal probability with and without the binding protein ParR. (G) ParM filaments with a *parC*-Au particle close to or touching the filament side (M with Au close to side) were observed with near equal probability with and without ParR. (H) Uncapped ParM filaments with no Au particles close by (M alone) were observed both with and without ParR. (I) Normalized histogram (occurrence divided by total number of filaments counted) of observed structures when monoconjugate *parC*-Au, ParM, and ATP are combined with and without ParR. Scale bar: 50 nm.

Figure 3. Measurement of the widths of ParM structures in various relationships with *parC*-Au/ParR particles demonstrates that the binding capacity of the ParR/*parC* complex is a single ParM filament. Filament widths in (A) Au-M structures, 53 total measured and (B) Au-M-Au structures, 27 total measured. In both types of structures, an average width of 6 nm is observed, in agreement with the accepted width for single ParM filaments.

Figure 4. Multiconjugate *parC*-Au/ParR particles (four or more *parC* DNA per Au particle) interact with bundles containing multiple ParM filaments. (A) Multiconjugate *parC*-Au (schematic) was used to investigate filament binding behavior to multiple *parC*. (B)-(E) ParM bundles with a *parC*-Au/ParR complex at one or both ends. Scale bar: 50 nm.

Figure 1

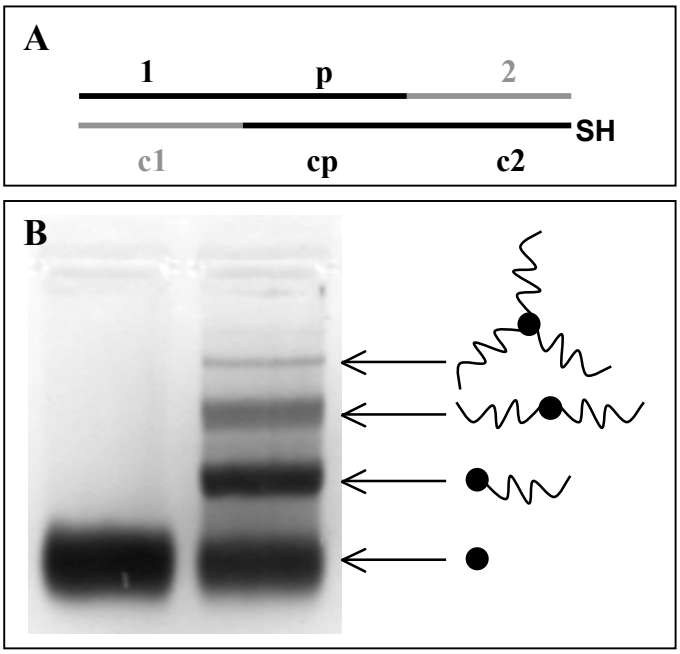

Figure 2

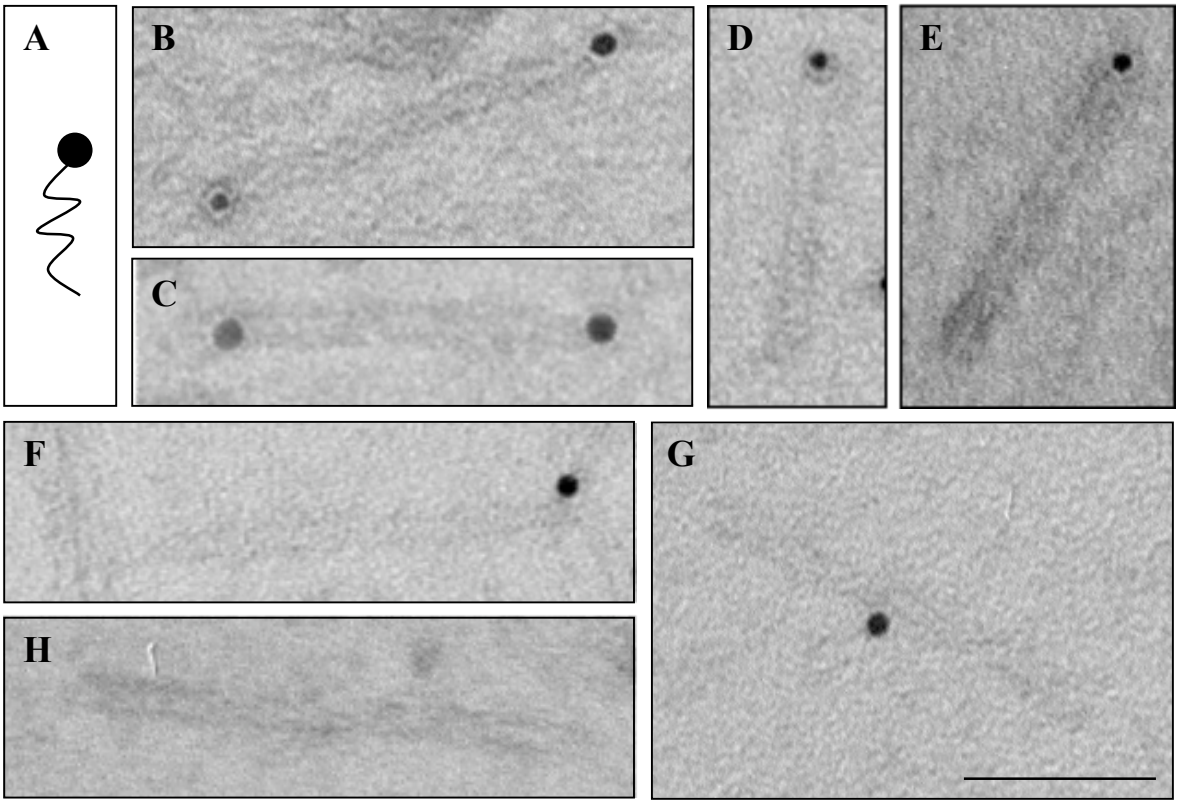
A
B
C
D
E
F
G
H

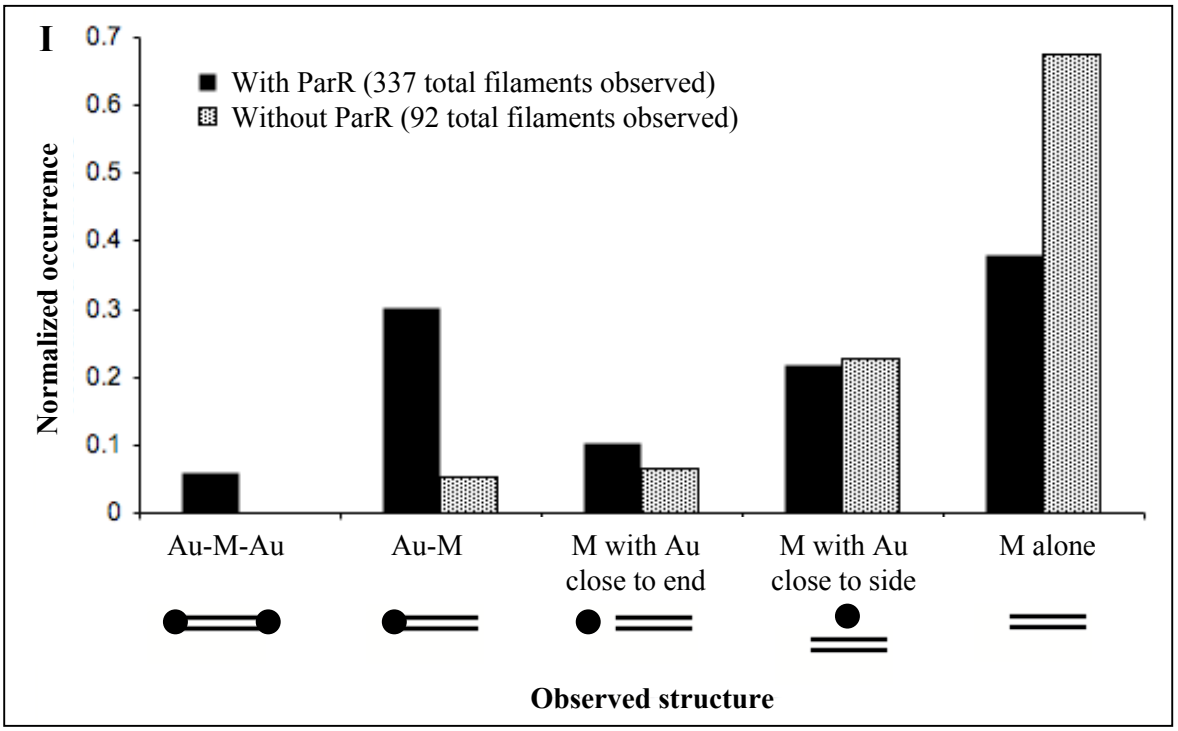
I
With ParR (337 total filaments observed)
Without ParR (92 total filaments observed)
Normalized occurrence
0.7
0.6
0.5
0.4
0.3
0.2
0.1
0
Au-M-Au
Au-M
M with Au close to end
M with Au close to side
M alone
Observed structure

Figure 3

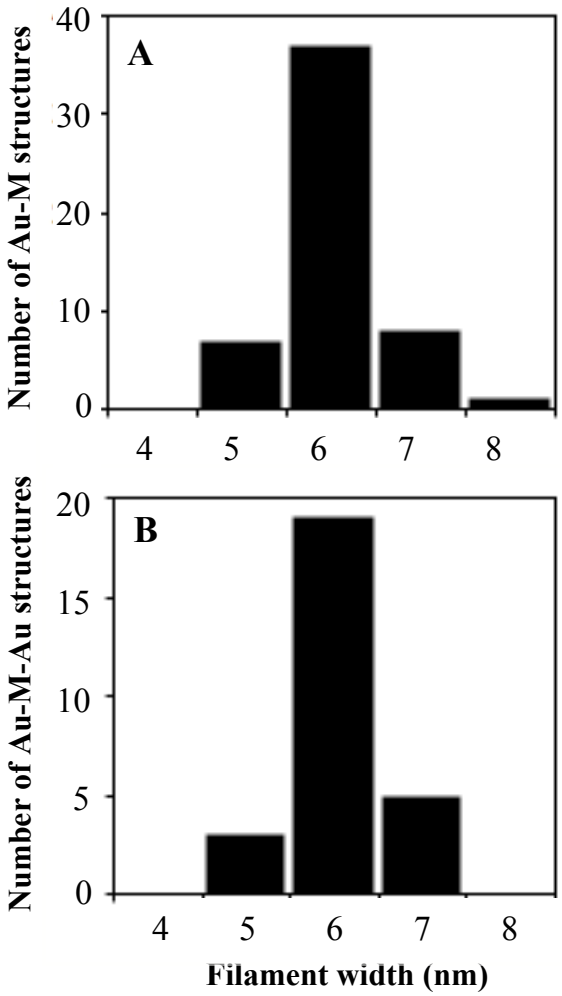
A
Number of Au-M structures
40
30
20
10
0
4
5
6
7
8
B
Number of Au-M-Au structures
20
15
10
5
0
4
5
6
7
8
Filament width (nm)

Figure 4